

# A Theoretical Investigation of Transport Layer-Free Homojunction Perovskite Solar Cells via a Detailed Photoelectric Simulation

Yuqi Zhang, Zhenhai Yang,\* Tianshu Ma, Zhenhai Ai, Changlei Wang, and Xiaofeng Li\*


Although the conventional n-i-p or p-i-n perovskite solar cells (PSCs) can produce ultrahigh efficiency (>25%), complex synthesis/deposition processes together with strict requirements for preparing the hole- and electron-transport layers (HTLs and ETLs) pose a challenge to accessing low-cost perovskite devices. To address this issue, a simple strategy of employing a self-doped perovskite homojunction to replace the HTLs and ETLs has been widely proposed. However, this type of TL-free homojunction PSCs is usually endowed with poor efficiency. Here, the design principles and working mechanisms of the TL-free homojunction PSCs are clarified via a rigorous photoelectric simulation. The potential of this type of device is unlocked by optimizing the structural/electrical parameters including thickness, doping concentration, bulk/interface defect concentration, contact barrier, and mobility of n-perovskite and p-perovskite. To further uncover the intrinsic physical behavior, ion migration, and photon recycling effects on this type of TL-free homojunction PSCs are also studied. In addition, devices with different types of structures including TL-free inverted, ETL-free, and HTL-free designs are briefly discussed. Finally, a clear roadmap for the promotion of device efficiency is proposed, providing valuable guidance for designing high-efficient TL-free homojunction PSCs.

## 1. Introduction

Perovskite solar cells (PSCs) have attracted much attention in the past decade due to their ever-increasing power conversion efficiencies (PCEs) together with low-cost potential.<sup>[1–7]</sup> Through an intensive worldwide effort, perovskite devices have

Y. Zhang, Z. Yang, T. Ma, Z. Ai, C. Wang, X. Li  
School of Optoelectronic Science and Engineering & Collaborative  
Innovation Center of Suzhou Nano Science and Technology  
Key Lab of Advanced Optical Manufacturing Technologies  
of Jiangsu Province & Key Lab of Modern Optical  
Technologies of Education Ministry of China  
Soochow University  
Suzhou 215006, China  
E-mail: yangzhenhai@nimte.ac.cn; xfli@suda.edu.cn

Z. Yang  
Ningbo Institute of Materials Technology and Engineering  
Chinese Academy of Sciences  
Ningbo 315201, China

 The ORCID identification number(s) for the author(s) of this article can be found under <https://doi.org/10.1002/aenm.202203366>.

DOI: 10.1002/aenm.202203366

recently received a new world record efficiency of 25.7%, approaching that of the mainstream crystalline silicon (c-Si) SCs (26.7%).<sup>[8]</sup> However, the full potential of this type of perovskite device especially in the photovoltaic (PV) industry has not yet been realized, which needs to rely on ongoing progresses to further boost the device efficiency while maintaining/lowering the manufacturing costs with the purpose of accelerating their industrialization process and enhancing their competitiveness in the PV community. In terms of the conventional n-i-p (or p-i-n) sandwich PSCs, device efficiency depends on the electron/hole transport layers (ETLs/HTLs) to offer a driving force for charge-carrier transport and extraction.<sup>[9]</sup> Even though a large number of ETLs and HTLs, such as TiO<sub>2</sub>, SnO<sub>2</sub>, and Spiro-OMeTAD, have been widely developed to construct the high-efficient PSCs, complex synthesis/deposition processes together with strict requirements for the preparation conditions pose a challenging to obtain the low-cost perovskite devices, which

thus appeals for the structural innovations to simplify the device designs.<sup>[10–12]</sup>

Inspired by the high-efficient c-Si solar cells, which usually fabricate a heavily doped p-type (or n-type) emitter on an n-type (or p-type) c-Si substrate to form a p<sup>+</sup>/n (or n<sup>+</sup>/p) homojunction, researchers have made many attempts to construct the self-doping perovskite by means of regulating perovskite component and annealing engineering, thus offering a chance to fabricate p-n homojunction/heterojunction PSCs.<sup>[13–15]</sup> The homojunction design has been considered to be a feasible strategy for the perovskite devices, which has been confirmed by a large number of simulations (Table S1, Supporting Information) and experiments. For instance, Cui et al. reported a FA<sub>0.15</sub>MA<sub>0.85</sub>PbI<sub>3</sub> homojunction PSC formed by a solution-processed n-type perovskite covered by a thermally evaporated p-type perovskite, which received an outstanding efficiency of 21.38%. Moreover, the continuous success of the perovskite self-doping technology also makes it possible for PSCs to access high efficiency even if transport layers (TLs) are absent. In terms of the TL-free PSCs, the built-in potential formed by the perovskite homojunction/heterojunction provides the devices with a driving force to address the processes of charge-carrier

separation, transport, and extraction, meaning that the perovskite devices, even without TLs, still could efficiently operate. For proof-of-concept purposes, Cui et al. presented a TL-free PSC with an efficiency of 8.08%.<sup>[16]</sup> Li et al. demonstrated a bandgap-graded p-n homojunction PSC by introducing a three-step dynamic spin-coating strategy to regulate the valence Sn distribution, which produced a 10.3% efficiency for a TL-free perovskite device.<sup>[17]</sup> In addition, Yang et al. reported a FAPbI<sub>3</sub>/MAPbI<sub>3</sub> heterojunction TL-free PSC prepared by a solution-processed method, yielding a remarkable efficiency of 16.57%, which is the highest efficiency for the TL-free PSCs so far.<sup>[18]</sup> Unfortunately, the efficiency of these TL-free PSCs is too low to be compared with that of the traditional high-efficient perovskite devices at the current stage, suggesting that although the absence of TLs could simplify the fabrication processes, the TL-free PSCs are usually achieved at the expense of sacrificing the device efficiency. In addition to the limitations of the fabrication processes, the poor efficiency of the TL-free PSCs is often associated with suboptimal design schemes and unclear working mechanisms. Therefore, design principles and underlying mechanisms of this type of TL-free PSCs that are conducive to deepening our understanding on such a device and guiding the promotion of device efficiency, are urgently needed.

To unlock the full potential of the TL-free homojunction PSCs, we clarify the design principles and working mechanisms of such a device by performing a numerical simulation. The performance of this type of TL-free homojunction PSCs is thoroughly evaluated by addressing the structural/electrical parameters, which include thickness, doping concentration, defect concentration, carrier mobility, contact barrier, etc. The simulation results suggest that: 1) the best thicknesses and doping concentrations for the n-perovskite/p-perovskite are determined to be 125/2500 nm and  $4 \times 10^{15}/10^{17} \text{ cm}^{-3}$ , respectively; 2) defects inside the p-perovskite and in the transparent conductive oxide (TCO)/n-perovskite interface are confirmed to be the important factors limiting the device performance; 3) carrier mobility for the n-perovskite should be well-regulated to avoid the efficiency roll-off; 4) an energy cliff, especially for the TCO/n-perovskite contact is beneficial to promote the device performance. In addition, ion migration and photon recycling (PR) effects are also investigated to reveal the underlying physical behavior of this type of TL-free homojunction PSCs. Moreover, devices with different types of structures including TL-free inverted, ETL-free, and HTL-free designs are briefly studied. Finally, a clear route map for the promotion of device efficiency is proposed, providing a feasible scheme to boost the efficiency of the TL-free homojunction PSCs to 24%.

## 2. Results and Discussion

### 2.1. Dependence of Thickness and Doping Concentration

The simulation model of the TL-free perovskite devices consisting of a TCO, a n-type, and a p-type CH<sub>3</sub>NH<sub>3</sub>PbI<sub>3</sub> perovskite layer as well as an Au electrode, is illustrated in Figure 1b, where the conventional structure with the double-sided TLs is presented in Figure 1a as a comparison. Since the TL-free PSCs rely on the p-n homojunction formed by the

n-type and p-type perovskite to offer a driving force for carrier transport and extraction, the doping concentrations for both n-perovskite ( $N_{\text{per}}$ ) and p-perovskite ( $P_{\text{per}}$ ) that determine the intensities of the built-in potential and electric field are thus particularly vital for this type of devices to achieve high performance. In addition, as another crucial factor in affecting the device performance, the thicknesses of n-perovskite ( $d_{\text{n}}$ ) and p-perovskite ( $d_{\text{p}}$ ) that govern the photogeneration and the transport length of charge carriers should be well designed. In this study, the impact of thicknesses and doping concentrations of perovskite layers on the device performance is first investigated by numerical simulations. By performing the optical simulation, the profiles of spatial carrier generation rate and the corresponding photo-current density can be obtained as shown in Figure S1 (Supporting Information) and Figure 1c. Figure 1c shows the dependence of perovskite thickness on the photo-current density of PSCs. Obviously, with the increase of perovskite thickness from 300 to 3100 nm, the photo-current density of PSCs increases rapidly first and then tends to be stable, meaning that increasing perovskite thickness contributes to boost the photo-current density of PSCs.

The electrical stimulation is then carried out to address the relationship between the thicknesses of n-type and p-type perovskite and the device PCEs. It is easy to find from Figure 1d that the high PCE values can be achieved by a thin n-perovskite (<200 nm) in combination with a thick p-perovskite (>1500 nm), yielding the optimal n-perovskite thickness of 125 nm, in line with the experimental results reported in the literature.<sup>[18]</sup> To further confirm this conclusion, the typical current-voltage ( $J$ - $V$ ) curves are plotted in Figure 1e,f, which suggest that: 1) if the p-perovskite thickness is fixed at 2500 nm as shown in Figure 1e, PSCs with a thin n-perovskite (100 nm) show a lower  $V_{\text{oc}}$ , and a thick n-perovskite one (300 nm) displays a poor FF, which can be confirmed by the related simulation results in Figure S2 (Supporting Information); 2) if the n-perovskite thickness is fixed at 100 nm as shown in Figure 1f, a thicker p-perovskite is beneficial to promote the device PCE by boosting the current density of devices due to the sufficient light absorption and the higher photo-current density as can be seen in Figure 1c.

In addition to the thickness, the doping concentration and type of perovskite can also be accurately regulated through experiments.<sup>[14,15]</sup> Therefore, based on the optimal  $d_{\text{n}}$  (i.e., 125 nm) and  $d_{\text{p}}$  (i.e., 2500 nm), the influence of  $N_{\text{per}}$  and  $P_{\text{per}}$  on device efficiency is then emphatically studied. The PCE contour shown in Figure 1g reveals that a hotspot of PCE located at the region of  $10^{15} \text{ cm}^{-3} < N_{\text{per}} < 10^{16} \text{ cm}^{-3}$  and  $10^{16} \text{ cm}^{-3} < P_{\text{per}} < 10^{18} \text{ cm}^{-3}$  can be observed, leaving behind the optimal  $N_{\text{per}}$  of  $\approx 4 \times 10^{15} \text{ cm}^{-3}$  and  $P_{\text{per}}$  of  $\approx 10^{17} \text{ cm}^{-3}$ . In order to further understand the variation of PCE with  $N_{\text{per}}$  and  $P_{\text{per}}$ , the representative  $J$ - $V$  curves are plotted in Figure 1h,i. It can be seen from Figure 1h that for a fixed  $P_{\text{per}}$  of  $10^{16} \text{ cm}^{-3}$ , increasing  $N_{\text{per}}$  could effectively boost  $V_{\text{oc}}$ , but it will lead to a reduced  $J_{\text{sc}}$ , especially for the cases with a high  $N_{\text{per}}$  (i.e.,  $>10^{17} \text{ cm}^{-3}$ ). The increased  $V_{\text{oc}}$  can be attributed to the enhanced built-in potential. However, increasing the doping concentration of perovskite will lower the width of the depletion region and reduce the electric field strength inside the n-perovskite region as shown in Figure S3b (Supporting Information). Since the

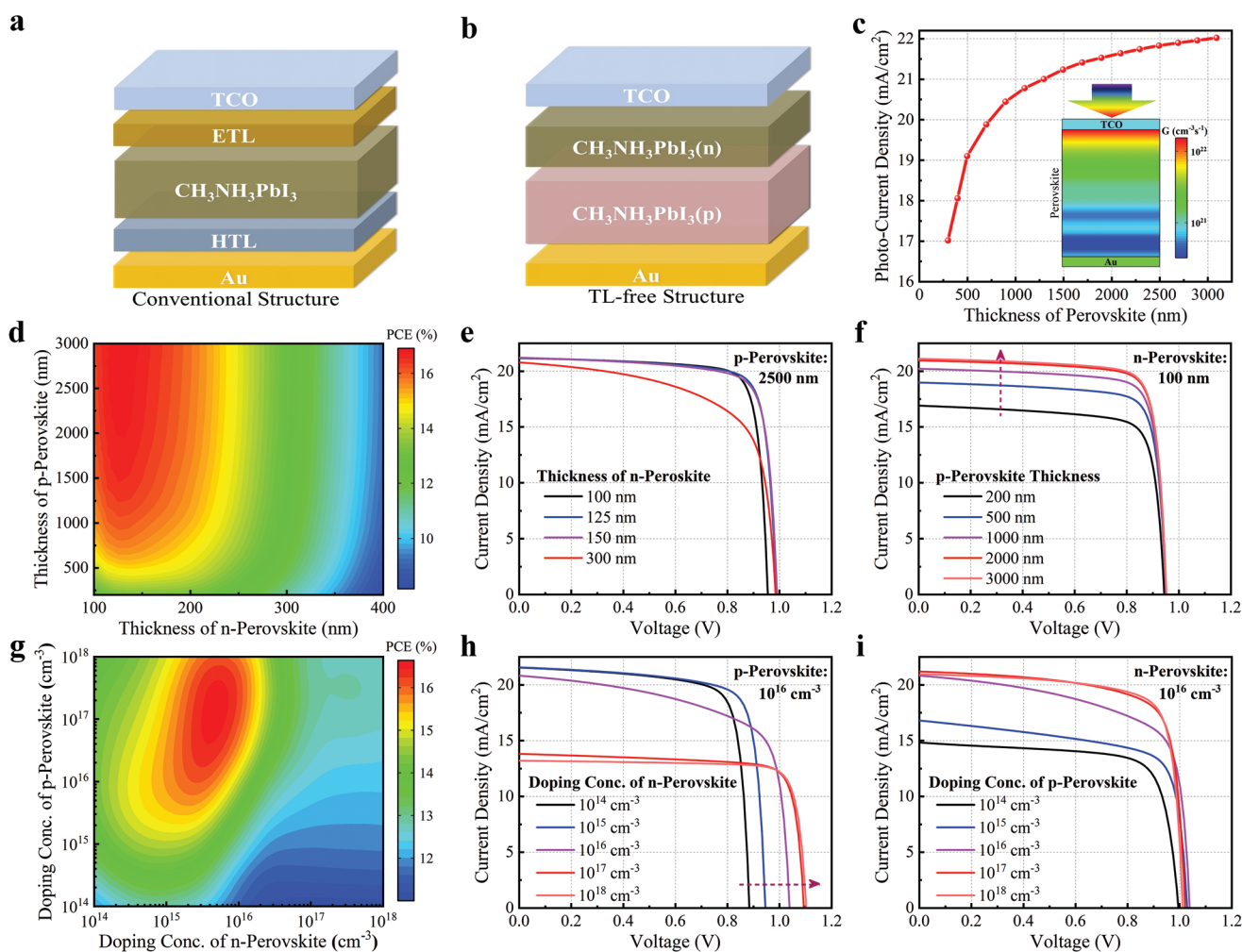


**Figure 1.** Schematic diagrams of perovskite devices with a) a conventional structure and b) a TL-free homojunction structure. c) Photo-current density of PSCs as a function of perovskite thickness, where the 2D profile of the carrier generation rate for a 1000 nm-thick perovskite is inserted in this figure. d) Contour of  $PCE$  values of PSCs under the various thicknesses of n-perovskite and p-perovskite, and the corresponding  $J-V$  curves under the typical e)  $d_n$  and f)  $d_p$ . g) Contour of  $PCE$  values of PSCs under the various  $N_{per}$  and  $P_{per}$ , and the corresponding  $J-V$  curves under the typical h)  $N_{per}$  and i)  $P_{per}$ . Here, an ideal Ohmic contact is considered.

generated carriers are concentrated in the n-type perovskite region, a poor electric field inside this region is unfavorable for carrier separation and transport, thus increasing the bulk and interface recombination and reducing  $J_{sc}$ . If  $N_{per}$  is fixed at  $10^{16} \text{ cm}^{-3}$  as shown in Figure 1i, the variation in  $P_{per}$  has less effect on  $V_{oc}$ , but it will boost  $J_{sc}$ . Different from the cases with the fixed  $P_{per}$  in Figure 1h, increasing  $P_{per}$  is conducive to promote the electric field strength of the n-perovskite depletion region, and thus facilitates the separation and transport of charge carriers, so that a high  $J_{sc}$  can be obtained.

## 2.2. Dependence of Bulk/Interface Defects and Carrier Mobility

Non-radiative recombination caused by bulk and interface defects has always been one of the most vital factors limiting device performance, which will be investigated in a detailed manner in this section. The simulation results are demonstrated in Figure 2, for which we can conclude that: i) as shown

in Figure 2a, the device  $PCE$  can be well-maintained until the defect concentration of TCO/n-perovskite interface ( $N_{it}$ ) is larger than  $10^{18} \text{ cm}^{-3}$ . The efficiency degradation for a high  $N_{it}$  case is mainly attributed to the decreased  $V_{oc}$ , which can be confirmed by the corresponding  $J-V$  curves in Figure 2b. The energy band structures shown in Figure S4a (Supporting Information) reveal that a high  $N_{it}$  will lead to a negative energy band bending and thus a reduced  $V_{oc}$ , which has been widely confirmed by many reports;<sup>[19]</sup> ii) the device  $PCE$  is almost independent of the defect concentration of Au/p-perovskite interface ( $P_{it}$ ) with the appearance of the identical  $J-V$  plots under the various  $P_{it}$  as shown in Figure 2c. This conclusion can be attributed to the fact that the presence of homojunction could effectively separate the charge carriers, and the electrons could be efficiently extracted by the top-side TCO electrode due to the shorter transport length inside the perovskite layer, leading to a low electron concentration in the p-perovskite region as shown in Figure S5 (Supporting Information) and thus negligible recombination in the Au/Perovskite interface even if the

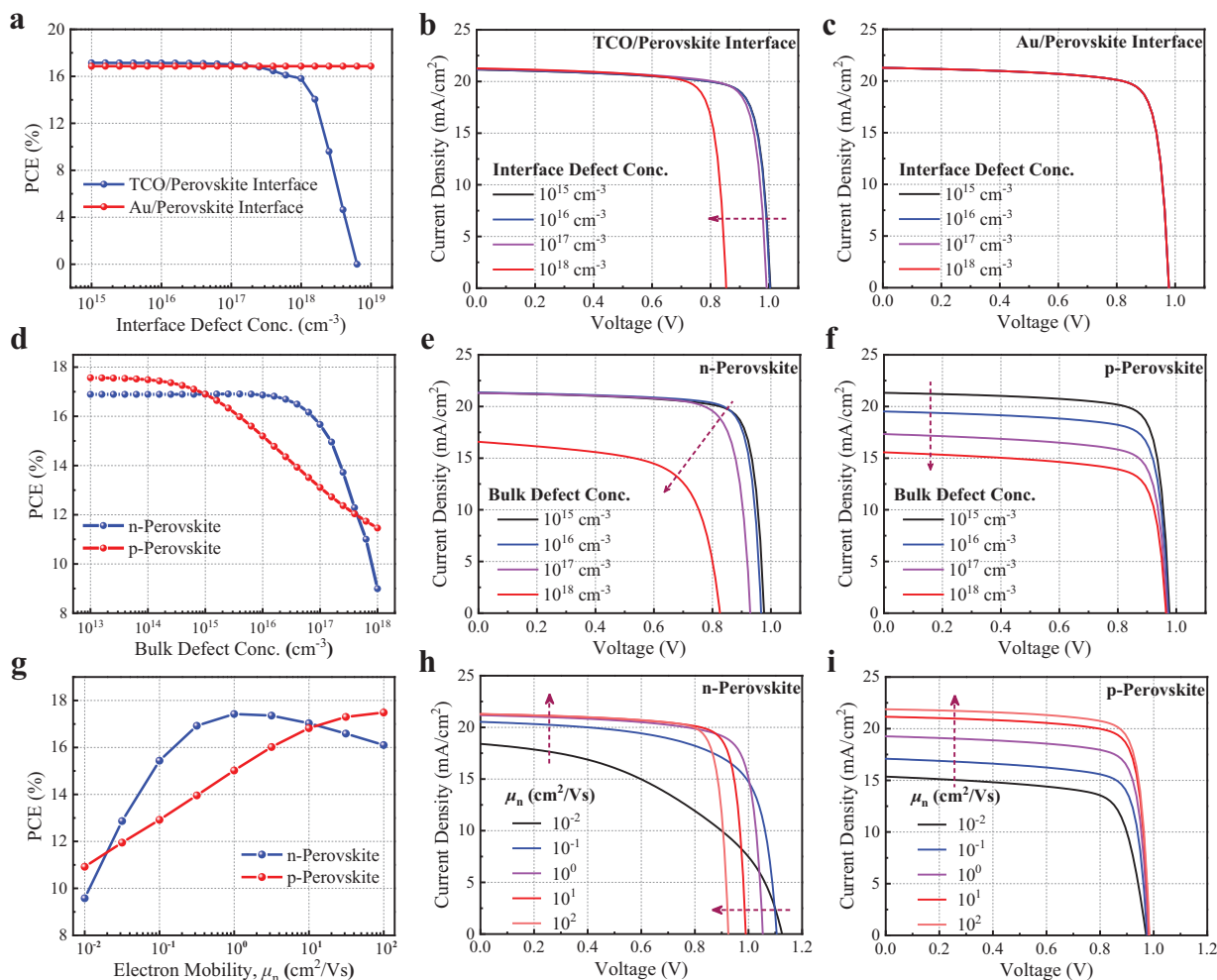


**Figure 2.** a) Dependence of  $N_{it}$  and  $P_{it}$  on device performance, and the corresponding  $J$ - $V$  curves under four typical b)  $N_{it}$  and c)  $P_{it}$ . d) Dependence of  $N_t$  and  $P_t$  on device performance, and the corresponding  $J$ - $V$  curves under four typical e)  $N_t$  and f)  $P_t$ . g) The effect of  $\mu_n$  ( $\mu_p = \mu_n/2$ ) for both n-perovskite and p-perovskite on device performance, and the corresponding  $J$ - $V$  curves under the different  $\mu_n$  for h) n-perovskite and i) p-perovskite. Here,  $d_n$  ( $d_p$ ),  $N_{per}$  ( $P_{per}$ ), and  $N_t$  ( $P_t$ ) are fixed at 125 (2500) nm,  $4 \times 10^{15}$  ( $1 \times 10^{17}$ )  $\text{cm}^{-3}$ , and  $10^{15}$  ( $10^{15}$ )  $\text{cm}^{-3}$ , respectively.

interface defect concentration is high enough (approaching  $10^{19} \text{ cm}^{-3}$ ). Therefore, it is crucial for this type of TL-free PSCs to passivate the TCO/n-perovskite interface other than the Au/p-perovskite interface; iii) as shown in Figure 2d, the device  $PCE$  has a tendency to remain unchanged first under  $N_t$  ( $P_t$ )  $< 10^{16}$  ( $10^{14}$ )  $\text{cm}^{-3}$  and then decrease rapidly under  $N_t$  ( $P_t$ )  $> 10^{17}$  ( $10^{15}$ )  $\text{cm}^{-3}$ , meaning that a high bulk defect in both n-perovskite and p-perovskite regions would degrade the device performance, and the n-perovskite has a high tolerance to the bulk defects due to the relatively thin thickness compared with that of the p-perovskite. The representative  $J$ - $V$  curves are plotted in Figure 2e,f, which suggest that: 1) the increase of  $N_t$  from  $10^{15}$  to  $10^{18} \text{ cm}^{-3}$  would lead to a decrease in  $V_{oc}$ , but the degradation of  $J_{sc}$  only occurs when  $N_t$  is high enough (i.e.,  $> 10^{17} \text{ cm}^{-3}$ ). The distributions of bulk recombination of the perovskite layers under the different  $N_t$  are demonstrated in Figure S4c (Supporting Information), hinting that a higher  $N_t$  would result in higher bulk recombination; 2) with the increase of  $P_t$  from  $10^{15}$

to  $10^{18} \text{ cm}^{-3}$ , a reduced  $J_{sc}$  can be observed, which can be attributed to the increased bulk recombination as can be confirmed by the recombination profiles in Figure S4d (Supporting Information). In a word, to achieve the high-efficient TL-free PSCs, the defects inside the p-perovskite and in the TCO/n-perovskite interface should be well-controlled.

Moreover, the impact of the charge carrier mobility on the device performance is then checked. The simulation results are shown in Figure 2g, which reveal that increasing carrier mobility is beneficial to promote the device's performance. In detail, the typical  $J$ - $V$  curves plotted in Figure 2h,i suggest that  $J_{sc}$  for the n-perovskite/p-perovskite case has an increasing trend with the increase of electron mobility ( $\mu_n$ ) from 0.01/0.01 to 1/100  $\text{cm}^2 \text{ Vs}^{-1}$ , manifesting that elevating carrier mobility could accelerate the transport and extraction of charge carriers, thus effectively suppressing the bulk/interface recombination and boosting the current density of devices. Interestingly, we observe an abnormal phenomenon from Figure 2g that the



*PCE* for the n-perovskite case has a downward trend with the increase of  $\mu_n$  from 1 to 100  $\text{cm}^2 \text{V}^{-1}\text{s}^{-1}$ . After careful observation of the  $J$ - $V$  curves in Figure 2h, we can find that case with a higher  $\mu_n$  shows a lower  $V_{oc}$ , which is also the main reason for the *PCE* roll-off. This conclusion is consistent with the previous reports.<sup>[20]</sup> For a low forward bias voltage, the drift current induced by the built-in electric field is so strong that it could minimize the local accumulation of charge carriers, so a high  $J_{sc}$  can be achieved regardless of carrier mobility. However, with the increase of the forward bias voltage, the built-in electric field is weakened, and the charge carrier transport behavior is dominated by the diffusion manner. In that case, higher carrier mobility means a stronger carrier diffusion, leading to the formation of an unfavorable potential bending as shown in Figure S6 (Supporting Information).

### 2.3. Contact Barrier Regulation

The abovementioned discussions are based on the assumption of an ideal Ohmic contact at the TCO/n-perovskite and Au/p-perovskite interfaces. In this section, the effect of the contact barrier ( $\Delta\phi$ ) on the device performance will be thoroughly investigated. The energy band diagrams of this type of TL-free homojunction perovskite devices are shown in Figure 3a, which suggest that a positive/negative contact barrier at the TCO/n-perovskite ( $\Delta\phi_n$ ) and Au/p-perovskite ( $\Delta\phi_p$ ) interfaces forms an energy spike/cliff for charge carrier transport. The relationship between  $\Delta\phi$  and the device *PCE* is detailed checked with

the corresponding results demonstrated in Figure 3b. It is easy to find from Figure 3b that: i) with the decrease of  $\Delta\phi_n$  from 0.6 to  $-0.4$  eV, the device *PCE* (blue line) shows a monotonically increasing trend, meaning that a relatively high energy cliff at the TCO/n-perovskite interface is helpful to promote the device performance; ii) the device *PCE* is almost insensitive to the contact barrier when  $\Delta\phi_p < 0.2$  eV, but it will be degraded only if  $\Delta\phi_p > 0.3$  eV, which implies that regulating contact barrier of the TCO/n-perovskite interface is more efficient for promoting the efficiency of the TL-free homojunction perovskite devices.

Moreover, the representative  $J$ - $V$  curves for both front and back contacts are also presented in Figure 3c,d. Obviously, a highly positive  $\Delta\phi_n$  (i.e., 0.4 eV) at the TCO/n-perovskite interface will greatly pull down the device  $V_{oc}$  due to the formation of an unfavorable energy band bending as shown in Figure S7a (Supporting Information). Since the optimal  $N_{per}$  as mentioned above is determined to be only  $\approx 4 \times 10^{15} \text{cm}^{-3}$ , which is so low that the energy band structure can be easily pulled when a positive or a negative contact barrier is applied at the TCO/n-perovskite interface, device  $V_{oc}$  is thus prone to be affected by this contact barrier. However, the results in Figure 3d indicate that the contact barrier at the Au/p-perovskite interface will not significantly alter the device  $J_{sc}$  and  $V_{oc}$ , but it will observably degrade the device *FF* if a highly positive  $\Delta\phi_p$  is applied. Because the doping concentration of p-perovskite is high enough (i.e.,  $\approx 10^{17} \text{cm}^{-3}$ ), the variation of the contact barrier at the Au/p-perovskite interface has less effect on the energy level alignment in the p-perovskite region, but it will form an energy spike/cliff to hinder/promote the transport of holes for

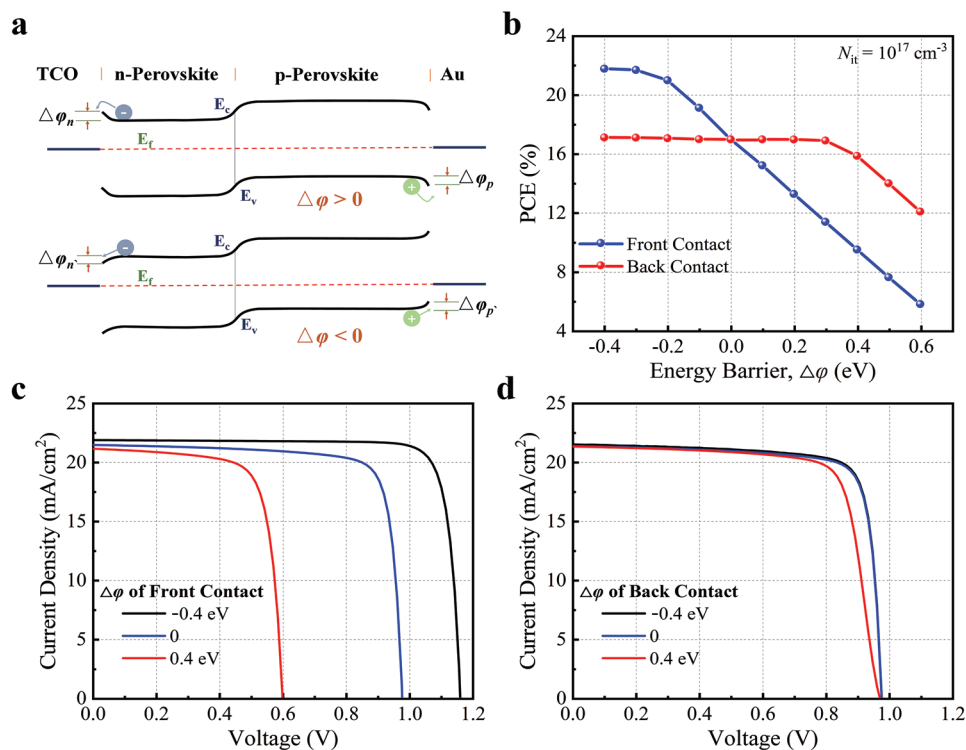


**Figure 3.** a) Energy band diagrams of TL-free perovskite structures for cases of  $\Delta\phi > 0$  and  $\Delta\phi < 0$ . b) *PCE* as a function of  $\Delta\phi$  for both front and back contacts under  $N_{it} = 10^{17} \text{cm}^{-3}$ , and the corresponding  $J$ - $V$  curves for c) front and d) back contacts under three representative  $\Delta\phi$ , that is,  $-0.4$ ,  $0$  and  $0.4$  eV.

a positive/negative contact barrier, thus resulting in an almost constant on  $J_{sc}$  but a degraded/increased  $FF$ . Here, it needs to be emphasized that devices with a highly negative contact barrier at the TCO/n-perovskite interface show a high  $PCE$  value approaching 22% under  $\Delta\phi_n = -0.4$  eV as shown in Figure 3b, much higher than that of the normal case (i.e.,  $\Delta\phi_n = 0$ ), thus providing a facile and effective strategy to boost the efficiency of the TL-free homojunction PSCs. In practice, a feasible strategy of introducing an ultra-thin organic material such as a self-assembled monolayer between electrode/perovskite interfaces has been widely performed to remove interface barrier or tailor the work-function of the related materials.<sup>[21,22]</sup>

## 2.4. Ion Migration and Hysteresis

Ion migration that has been proven to be the primary reason for the emergence of hysteresis behavior has been widely studied in the traditional sandwich perovskite devices.<sup>[23–25]</sup> Driven by the built-in electric field, these movable ions will migrate inside the perovskite layer and then accumulate at the perovskite-related interfaces. Meanwhile, the process of the ion migration as well as these accumulated ions at the interfaces will also mediate carrier transport behavior by altering the spatial distributions of electric field and carrier concentrations, thus affecting the device performance. Therefore, it is of great significance to elaborate the process of ion migration and its effects on the performance of the TL-free homojunction PSCs. Energy band structures for cases of the none ion migration and ion migration are illustrated in Figure 4a,b, respectively, in

which the strength of ion migration is expressed by the average ion concentration ( $N_{ion}$ ) within the whole perovskite region.

First of all, to evaluate and quantify the hysteresis effect, a typical parameter, that is, Hysteresis Factor ( $HF$ ), that has been widely adopted, can be defined as:<sup>[23]</sup>

$$HF = \frac{PCE(R) - PCE(F)}{PCE(R)} \quad (1)$$

where  $PCE(R)/PCE(F)$  represents the  $PCE$  value measured under reverse/forward voltage scan. The simulated  $HF$  value under the various  $N_{ion}$  and the representative  $J-V$  curves are demonstrated in Figure 4c,d, respectively, which manifest that if  $N_{ion}$  is less than  $10^{16}$   $\text{cm}^{-3}$ , the hysteresis effect is not obvious with the appearance of a small  $HF$  value together with a small difference between reverse and forward  $J-V$  curves. However, with the  $N_{ion}$  increases to  $10^{17}$   $\text{cm}^{-3}$ , an obvious hysteresis phenomenon with a high  $HF$  value and a large gap between reverse and forward  $J-V$  curves can be seen.

Different from the traditional sandwich perovskite devices, this type of TL-free homojunction PSCs rely highly on the built-in electric field formed by the n-perovskite and p-perovskite to provide a driving force for carrier transport and ion migration. As shown in Figure 4e, the electric field strength in the n-perovskite layer is much higher than that in the p-perovskite layer, leading to that ion accumulation only occurs at the TCO/n-perovskite interface as shown in Figure 4e and Figure S8 (Supporting Information). Here, we need to point out that although ion migration will reduce the device  $V_{oc}$ , especially for the case of  $N_{ion} = 10^{17}$   $\text{cm}^{-3}$ , it could also promote

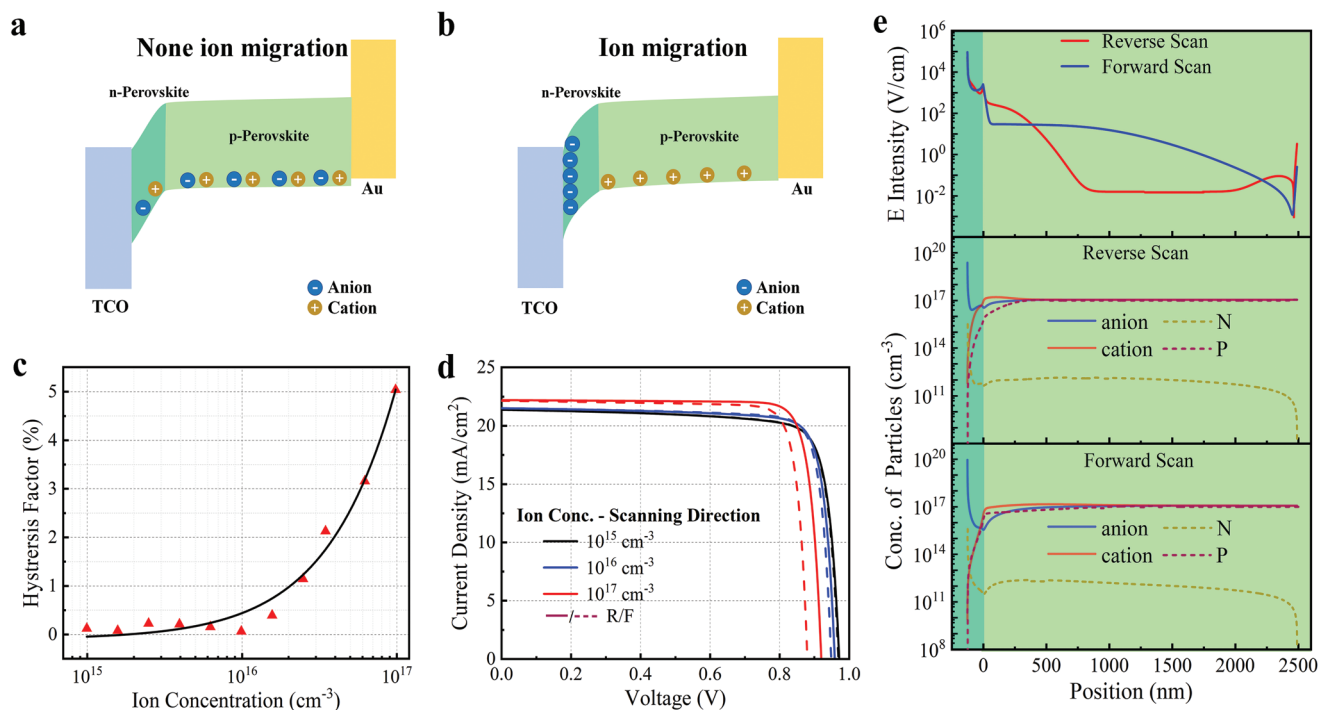


**Figure 4.** a) Schematic diagrams of energy band structures of TL-free homojunction PSCs for cases of a) non ion migration and b) ion migration. c) The relationship between ion concentration and  $HF$  value. d) The representative  $J-V$  curves under  $N_{ion} = 10^{15}$ ,  $10^{16}$  and  $10^{17}$   $\text{cm}^{-3}$ . e) E intensity and carrier/ion concentration profiles for reverse and forward scans under MPP-like conditions.

the device  $J_{sc}$  more or less. As shown in Figure S9 (Supporting Information), the variation in  $V_{oc}$  can be attributed to the change of energy band structures, and the improved  $J_{sc}$  for the case of  $N_{ion} = 10^{17} \text{ cm}^{-3}$  is due to the enhanced electric field intensity inside the p-perovskite region. This means that ion migration does not always have a negative impact on device performance.

## 2.5. Photon Recycling Effect

Photon recycling (PR) that refers to the multiple absorption-diffusion-emission processes has been widely studied in perovskite-based devices. It is well known that radiative recombination will dissipate energy by means of releasing photons, which will either escape from the device and/or be parasitically absorbed by the functional materials or electrodes, or be re-absorbed by perovskite layer and generate new electron-hole pairs, so as to achieve the purpose of re-using photons. Besides, the PR effect has been confirmed to have a positive impact on device performance by mitigating radiative recombination, which is particularly relevant for the cases with thick perovskite layers. Therefore, it is necessary to clarify the impact of the PR effect on the performance of TL-free homojunction perovskite devices.

As shown in Figure 5a, a detailed model is established to describe the PR processes for this type of TL-free homojunction

PSCs. It clearly shows that there are three possible routes for the emitted photons: i) be parasitically absorbed by the double-sided electrodes with a probability of  $P_a$ , ii) escape the device from the top surface with a probability of  $P_e$ , iii) be re-absorbed by the perovskite layer and generate new electron-hole pairs with a probability of  $P_r$ . For cases i) and ii), photons within the escape cones cannot be re-absorbed by the perovskite layer, and thus are absent from the PR processes. Here, both TCO and Au electrodes could cause parasitic absorption with the corresponding probabilities written as:<sup>[26]</sup>

$$P_{a\_TCO} = \frac{\int_{E_g}^{\infty} n_{TCO}^2 A_{front}(E) \phi_{bb}(E) dE}{\int_{E_g}^{\infty} 4n_{per}^2 d_{per} \alpha(E) \phi_{bb}(E) dE} \quad (2)$$

$$P_{a\_Au} = \frac{\int_{E_g}^{\infty} n_{Au}^2 A_{back}(E) \phi_{bb}(E) dE}{\int_{E_g}^{\infty} 4n_{per}^2 d_{per} \alpha(E) \phi_{bb}(E) dE} \quad (3)$$

where  $n_{TCO}$ ,  $n_{per}$  and  $n_{Au}$  are the real part of refractive indexes of TCO, perovskite, and Au, respectively,  $A_{front}$  and  $A_{back}$  are the absorbance of perovskite from the front- and back-sided illumination, respectively,  $d_{per}$  is the perovskite thickness,  $\alpha$  is the absorption coefficient of perovskite, and  $\phi_{bb}$  is the blackbody radiation flux. In the same way, the escape probability  $P_e$  can be written as:

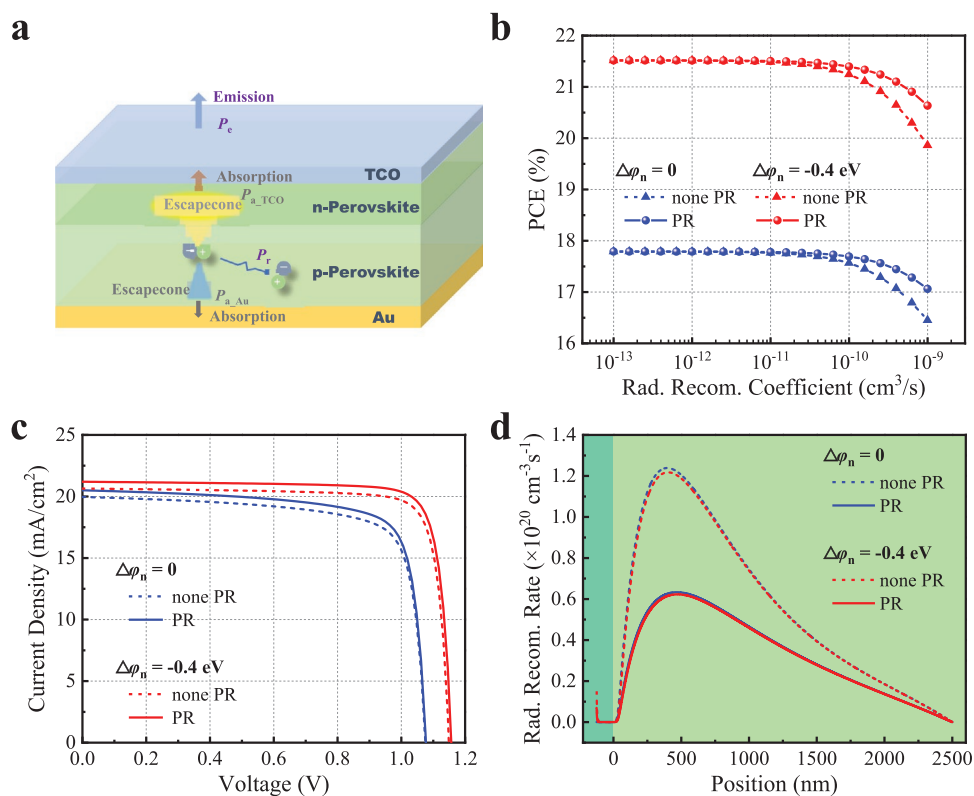


**Figure 5.** a) Sketch map of the possible routes of the remitted photons within the perovskite layer. b) Dependence of radiative recombination coefficient on device PCE under the different cases. c) The representative  $J$ - $V$  curves and d) the distributions of radiative recombination rate at the SC condition for the none PR and PR cases under  $\Delta\phi_n = 0$  and  $-0.4 \text{ eV}$  at the radiative recombination coefficient is equal to  $10^{-9} \text{ cm}^3 \text{ s}^{-1}$ .

$$P_e = \frac{\int_{E_g}^{\infty} n_{\text{TCO}}^2 A_{\text{front}}(E) \phi_{\text{bb}}(E) dE}{\int_{E_g}^{\infty} 4n_{\text{per}}^2 d_{\text{per}} \alpha(E) \phi_{\text{bb}}(E) dE} \quad (4)$$

The total parasitic absorption probability,  $P_a$ , can be calculated by

$$P_a = P_{a\text{-TCO}} + P_{a\text{-Au}} \quad (5)$$

thus, the re-absorbed probability,  $P_r$  can be expressed as:

$$P_r = 1 - P_a - P_e \quad (6)$$

By implementing the numerical simulations based on these equations, the vital parameters including  $P_e$ ,  $P_a$  and  $P_r$  can be extracted, which thus allows us to mediate the radiative recombination process and investigate the PR effect on the device performance. As strong evidence has been provided that the presence of PR would have a more obvious effect on promoting the device performance if the nonradiative recombination can be intrinsically suppressed, the case of  $\Delta\phi_n = -0.4$  eV with reduced nonradiative interface recombination is also included in this study.<sup>[26]</sup> This conclusion can be further confirmed by the radiative recombination distributions in Figure S10 (Supporting Information). The simulation results concerning the dependence of the radiative recombination coefficient on device  $PCE$  are displayed in Figure 5b. It can be concluded from this figure that for cases of  $\Delta\phi_n = 0$  and  $-0.4$  eV, the device  $PCE$  can be well-maintained until the radiative recombination coefficient

is larger than  $10^{-11} \text{ cm}^3 \text{ s}^{-1}$ , and an obvious  $PCE$  difference between none PR case and PR case can be observed under the radiative recombination coefficient is greater than  $10^{-10} \text{ cm}^3 \text{ s}^{-1}$ . This is due to the remarkable nonradiative recombination inherent to this type of TL-free homojunction PSCs is much higher than that of the radiative recombination, thus resulting in a limited recombination proportion for the case with a small radiative recombination coefficient.

The representative  $J-V$  curves under the radiative recombination coefficient of  $10^{-9} \text{ cm}^3 \text{ s}^{-1}$  are plotted in Figure 5c, which clearly indicate that the presence of PR could promote the device  $J_{sc}$ . It is somewhat contradictory to the widely accepted cognition that PR can effectively boost device  $V_{oc}$  other than  $J_{sc}$ .<sup>[27]</sup> In fact, this is easy to understand that the absence of TMs for this type of TL-free homojunction PSCs will lead to strong nonradiative and radiative recombination even under a small bias voltage, so introducing the PR will reduce radiative recombination and thus boost the device  $J_{sc}$ . Moreover, the distributions of radiative recombination rate under the different cases are plotted in Figure 5d, which confirms that the PR effect could effectively suppress radiative recombination.

## 2.6. Efficiency Promotion Strategy

In the last section, we briefly discuss the  $PCE$  variation under the different types of PSCs, including TL-free normal, TL-free inverted, ETL-free, and HTL-free structures as shown in Figure S11 (Supporting Information). The related parameters

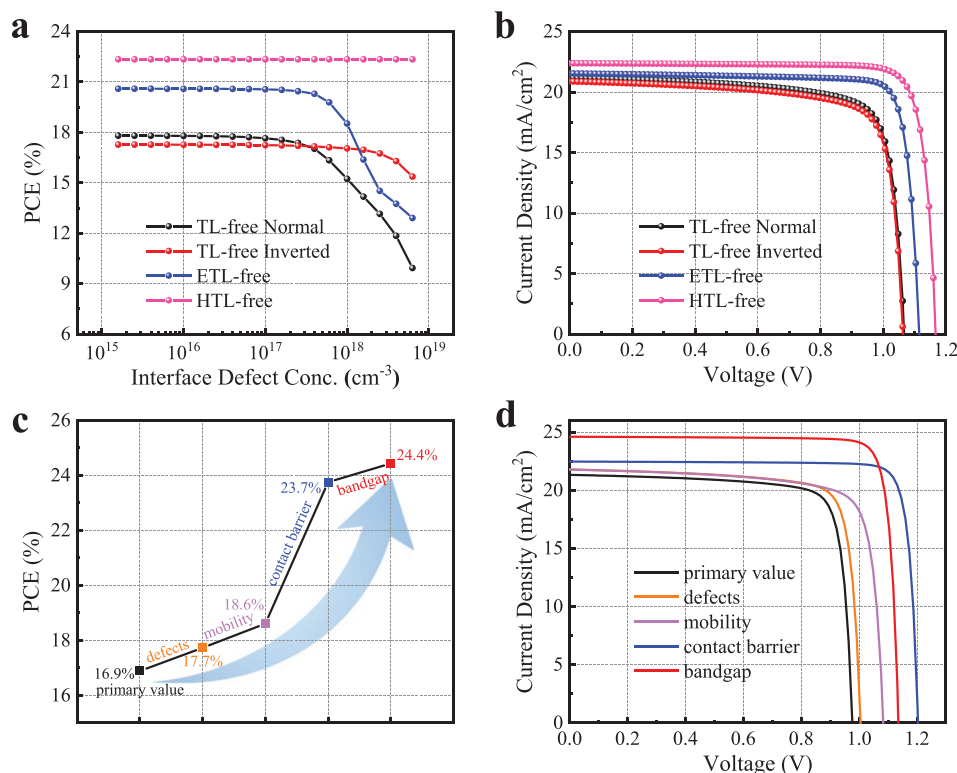


**Figure 6.** a)  $PCE$  values as a function of interface defect concentration of the four related devices, and b) the corresponding  $J-V$  curves under the interface defect concentration of  $10^{17} \text{ cm}^{-3}$ . c) A detailed roadmap for promoting the efficiency of TL-free PSCs, and d) the corresponding  $J-V$  curves.



used for this simulation are listed in Table S3 (Supporting Information). The relationship between the defect concentration of perovskite-related interfaces and the device *PCE* is shown in Figure 6a. It is apparent that devices with HTL-free and ETL-free structures show higher *PCE* values than that TL-free ones, indicating that the absence of the transport layers will degrade the device performance even if the interface defects are low enough. Moreover, it is worth noting that HTL-free devices show higher device performance than that of ETL-free devices, which can be attributed to the fact that the light is incident from the TCO side for this type of n-i-p perovskite devices, leading to carrier generation gathers on the front side of perovskite (Figure 1c), so the presence of ETL is conducive to promoting carrier transport and extraction. This is also the reason why HTL-free devices are almost independent of interface defect concentration. Moreover, the typical *J–V* curves for these four related devices under the interface defect concentration of  $10^{17} \text{ cm}^{-3}$  are plotted in Figure 6b, and the corresponding electrical parameters are listed in Table S4 (Supporting Information), which hint that the HTL-free and ETL-free devices show superior performance in  $J_{sc}$ ,  $V_{oc}$  and *FF* compared with the TL-free devices.

To further unlock the potential of TL-free PSCs, a clear roadmap for improving device performance is proposed as shown in Figure 6c which is summarized as follows: i) based on the optimized thickness (i.e., 125/2500 nm for n-perovskite/p-perovskite) and doping concentration (i.e.,  $4 \times 10^{15}/10^{17} \text{ cm}^{-3}$  for n-perovskite/p-perovskite), a primary *PCE* is determined to be 16.9%; ii) by suppressing the bulk and interface recombination with a low bulk defect concentration of  $10^{14} \text{ cm}^{-3}$ , and a low interface defect concentration of  $10^{17} \text{ cm}^{-3}$ , the *PCE* of this type of TL-free PSCs can be improved to 17.7%; iii) a higher *PCE* of 18.6% can be attained by regulating the electron mobility with a suitable mobility (i.e.,  $1/12.5 \text{ cm}^2 \text{ Vs}^{-1}$  for the n-perovskite/p-perovskite); iv) with the regulation of the contact barrier from 0 to  $-0.4 \text{ eV}$ , a remarkable *PCE* of 23.7% can be obtained; v) an excellent *PCE* of 24.4% can be expected by screening a suitable bandgap of perovskite as shown in Figure S12 (Supporting Information). Moreover, the corresponding *J–V* curves are plotted in Figure 6d, which indicate a superior  $J_{sc}$ ,  $V_{oc}$ , and *FF* for TL-free homojunction PSCs.

Although the current efficiency of this type of TL-free homojunction perovskite solar cells is still lower than that of the normal PSCs with TLs, it is expected to achieve a competitive efficiency with the continuous progress of preparation technology. More importantly, the absence of TLs for the TL-free homojunction perovskite solar cells could simplify the preparation processes and reduce fabrication costs, thus promoting the industrialization of perovskite-based devices.

In the last, we still need to emphasize the innovation of this work. First, the strictly optical coupled electrical simulation was realized by using the finite-element method, and the resulting results are thus considered to be more accurate and credible compared with that of 1D software. Second, a series of structural/electrical parameters including thickness, doping concentration, bulk/interface defect concentration, contact barrier, and mobility of n-perovskite and p-perovskite, etc., were synchronously optimized, providing a panorama of the correlation between parameters and device performance. Furthermore,

the intrinsic physical behavior of such a TL-free homojunction perovskite solar cell with the ion migration and photon recycling effects was clarified and produced many interesting conclusions.

### 3. Conclusion

In this study, we performed a rigorous photoelectrical simulation to clarify the design principles and working mechanisms of the TL-free homojunction PSCs. Through the investigation of a series of structural/electrical parameters including thickness, doping concentration, bulk/interface defect concentration, and mobility of n-perovskite and p-perovskite, the dependence of these parameters on device performance was elaborated in detail. The simulation results suggest that a homojunction formed by a thin and a low doped n-perovskite together with a thick and a high doped p-perovskite, a low interface/bulk defect concentration, and suitable mobility, are required for high-efficient TL-free PSCs. The effect of the contact barrier on device performance was checked, which hints that an energy cliff especially for the TCO/n-perovskite contact is beneficial to promote the device performance. Moreover, the process of ion migration and PR effects were also studied to uncover the underlying physical behavior of this type of TL-free homojunction perovskite device. Finally, TL-free inverted, ETL-free, and HTL-free devices were also briefly investigated, and a clear route map for the promotion of device efficiency was proposed, providing valuable guidance for designing high-efficient TL-free homojunction PSCs.

### 4. Experimental Section

In this study, the finite element method was used to perform the numerical simulations based on the platform of COMSOL Multiphysics. First, the accurate spatial distributions of the electromagnetic field were obtained by solving Maxwell's equations under AM 1.5G, so that the optical absorption and charge-carrier generation could be evaluated. Based on the distributions of carrier generation in the optical module, the electrical stimulation to address the transport/recombination/extraction processes of these carriers was then carried out by coupling Poisson's equation, carrier continuity equations, and drift-diffusion equations, which can be written as<sup>[26,28–30]</sup>

$$\nabla^2\Phi = (n - p + N_d - N_a) \quad (7)$$

$$\frac{\partial n}{\partial t} = \frac{1}{q} \nabla \cdot J_n + G - U; \quad \frac{\partial p}{\partial t} = -\frac{1}{q} \nabla \cdot J_p + G - U \quad (8)$$

$$J_n = qn\mu_n(-\nabla\Phi) + qD_n\nabla n; \quad J_p = qp\mu_p(-\nabla\Phi) - qD_p\nabla p \quad (9)$$

where  $\Phi$  is the electrostatic potential,  $n$  ( $p$ ) is the electron (hole) concentration,  $N_d$  ( $N_a$ ) is the donor (acceptor) doping concentration,  $q$  is the electron charge,  $J_n$  ( $J_p$ ) is the electron (hole) current density,  $G$  is the carrier generation rate,  $U$  is the carrier recombination rate,  $\mu_n$  ( $\mu_p$ ) is the electron (hole) mobility,  $D_n$  ( $D_p$ ) is the carrier diffusion coefficient. The key parameters used for this simulation are listed in Table S2 (Supporting Information). By solving these equations, the electrical parameters/properties including *J–V* characteristic curves and distributions of electric field, potential, carrier concentration, and carrier

recombination, etc., can be obtained. Besides, an ideal Ohmic contact was assumed for both the TL-free interfaces.

## Supporting Information

Supporting Information is available from the Wiley Online Library or from the author.

## Acknowledgements

This work was supported by the National Natural Science Foundation of China (Nos. 61875143, 62120106001, 62004199, and 62005188), Natural Science Foundation of Jiangsu Province (BK20190825), Priority Academic Program Development (PAPD) of Jiangsu Higher Education Institutions.

## Conflict of Interest

The authors declare no conflict of interest.

## Data Availability Statement

Research data are not shared.

## Keywords

homojunctions, perovskite solar cells, photoelectric simulation, transport layer-free

Received: October 5, 2022  
Revised: December 5, 2022  
Published online:

- [1] M. Jeong, I. W. Choi, E. M. Go, Y. Cho, M. Kim, B. Lee, S. Jeong, Y. Jo, H. W. Choi, J. Lee, *Science* **2020**, 369, 1615.
- [2] J. J. Yoo, G. Seo, M. R. Chua, T. G. Park, Y. Lu, F. Rotermund, Y. K. Kim, C. S. Moon, N. J. Jeon, J. P. Correa-Baena, V. Bulovic, S. S. Shin, M. G. Bawendi, J. Seo, *Nature* **2021**, 590, 587.
- [3] G.-H. Kim, D. S. Kim, *Joule* **2021**, 5, 1033.
- [4] J. Y. Kim, J.-W. Lee, H. S. Jung, H. Shin, N.-G. Park, *Chem. Rev.* **2020**, 120, 7867.
- [5] N.-G. Park, *J. Phys. Chem. Lett.* **2013**, 4, 2423.
- [6] S. Sajid, A. M. Elseman, H. Huang, J. Ji, S. Dou, H. Jiang, X. Liu, D. Wei, P. Cui, M. Li, *Nano Energy* **2018**, 51, 408.
- [7] Z. Song, C. L. McElvany, A. B. Phillips, I. Celik, P. W. Krantz, S. C. Waththage, G. K. Liyanage, D. Apul, M. J. Heben, *Energy Environ. Sci.* **2017**, 10, 1297.
- [8] M. A. Green, E. D. Dunlop, J. Hohl-Ebinger, M. Yoshita, N. Kopidakis, K. Bothe, D. Hinken, M. Rauer, X. Hao, *Prog. Photovoltaics* **2022**, 30, 687.
- [9] M. Cai, N. Ishida, X. Li, X. Yang, T. Noda, Y. Wu, F. Xie, H. Naito, D. Fujita, L. Han, *Joule* **2018**, 2, 296.
- [10] N. J. Jeon, H. G. Lee, Y. C. Kim, J. Seo, J. H. Noh, J. Lee, S. I. Seok, *J. Am. Chem. Soc.* **2014**, 136, 7837.
- [11] P. Wu, S. Wang, X. Li, F. Zhang, *J. Mater. Chem. A* **2021**, 9, 19554.
- [12] J. F. Liao, W. Q. Wu, Y. Jiang, J. X. Zhong, L. Wang, D. B. Kuang, *Chem. Soc. Rev.* **2020**, 49, 354.
- [13] D. Song, P. Cui, T. Wang, D. Wei, M. Li, F. Cao, X. Yue, P. Fu, Y. Li, Y. He, B. Jiang, M. Trevor, *J. Phys. Chem. C* **2015**, 119, 22812.
- [14] Q. Wang, Y. Shao, H. Xie, L. Lyu, X. Liu, Y. Gao, J. Huang, *Appl. Phys. Lett.* **2014**, 105, 163508.
- [15] P. Cui, D. Wei, J. Ji, D. Song, Y. Li, X. Liu, J. Huang, T. Wang, J. You, M. Li, *Sol. RRL* **2017**, 1, 1600027.
- [16] P. Cui, D. Wei, J. Ji, H. Huang, E. Jia, S. Dou, T. Wang, W. Wang, M. Li, *Nat. Energy* **2019**, 4, 150.
- [17] H. Sun, K. Deng, J. Xiong, L. Li, *Adv. Energy Mater.* **2020**, 10, 1903347.
- [18] X. Yang, Q. Li, Y. Zheng, D. Luo, Y. Zhang, Y. Tu, L. Zhao, Y. Wang, F. Xu, Q. Gong, R. Zhu, *Joule* **2022**, 6, 1277.
- [19] F. Izadi, A. Ghobadi, A. Gharaati, M. Minbashi, A. Hajjiah, *Optik* **2021**, 227, 166061.
- [20] H. Lee, A. Rana, I. Kyymissis, C.-H. Kim, *Sol. Energy* **2022**, 236, 473.
- [21] Y. Zhou, C. Fuentes-Hernandez, J. Shim, J. Meyer, A. J. Giordano, H. Li, P. Winget, T. Papadopoulos, H. Cheun, J. Kim, M. Fenoll, A. Dindar, W. Haske, E. Najafabadi, T. M. Khan, H. Sojoudi, S. Barlow, S. Graham, J. L. Bredas, S. R. Marder, A. Kahn, B. Kippelen, *Science* **2012**, 336, 327.
- [22] F. H. Isikgor, S. Zhumagali, L. V. T. Merino, M. De Bastiani, I. McCulloch, S. De Wolf, *Nat. Rev. Mater.* **2022**, <https://doi.org/10.1038/s41578-022-00503-3>.
- [23] J. Xiang, Y. Li, F. Huang, D. Zhong, *Phys. Chem. Chem. Phys.* **2019**, 21, 17836.
- [24] D. Lan, *Prog. Photovoltaics* **2019**, 28, 533.
- [25] Z. Ai, D. Wu, T. Ma, Y. Zhao, Y. An, C. Wang, X. Li, *Sol. RRL* **2022**, 6, 2200606.
- [26] Z. Yang, W. Yang, X. Yang, J. C. Greer, J. Sheng, B. Yan, J. Ye, *Energy Environ. Sci.* **2020**, 13, 1753.
- [27] T. Kirchartz, F. Staub, U. Rau, *ACS Energy Lett.* **2016**, 1, 731.
- [28] A. Shang, X. Li, *Adv. Mater.* **2017**, 29, 1603492.
- [29] Y. An, A. Shang, G. Cao, S. Wu, D. Ma, X. Li, *Sol. RRL* **2018**, 2, 1870227.
- [30] Y. An, C. Wang, G. Cao, X. Li, *ACS Nano* **2020**, 14, 5017.